Construction and Building Materials 351 (2022) 128954

Contents lists available at ScienceDirect

Construction and Building Materials

journal homepage: www.elsevier.com/locate/conbuildmat

Evaluation of carbon grid reinforcement in asphalt pavement

Sang-Yum Lee [a], Tam Minh Phan [b], Dae-Wook Park [b,*]

[a] Dept. of Civil Engineering, Induk University, Seoul 01878, South Korea
[b] Dept. of Civil Engineering, Kunsan National University, Gunsan-si 54150, Jeollabuk-do, South Korea

ARTICLE INFO

Keywords:
Asphalt mixture
Grid reinforcement
Grid efficiency factor
Pavement performance year
LCCA

ABSTRACT

This study aims to analyze the advantages of carbon grid reinforcement in asphalt pavement based on performance tests, pavement design, and life cycle cost analysis (LCCA). The improvement in mechanical property was examined by overlay tester (OT), four-point bending, Hamburg wheel tracking, and shear bond strength test. Grid efficiency factor (GEF) was computed to evaluate the enhancement of cracking resistance. Based on the OT results, the performance year was quantified by a mechanical-empirical model of reflective cracking rate. Then, the outcomes from the performance year analysis were used to determine the economic effect through 20-year service by life cycle cost analysis (LCCA). Overall, carbon grid reinforcement not only enhances the performance of asphalt mixture but also prolongs service life, thus beneficial in cost-effectiveness. For instance, the resistance to reflection cracking was improved; deformation and rutting velocity was reduced due to the presence of a grid layer; GEFs of grid reinforced mixtures ranged from 1.5 to 2.5. Finally, the asphalt mixture containing grid would increase performance year by 2–4 times than that of conventional asphalt mixture. Therefore, the total cost of the grid reinforced alternative was reduced by approximately 43% through a 20-year service.

1. Introduction

Asphalt pavement is widely used on roads due to its essential characteristics such as fast construction, reusability, smoothness, and noise absorption. The demand for use of asphalt mixture for paved roads has significantly increased over time. In South Korea, over 90 % of roadways were paved by asphalt mixture, this number in the United States exceeded 94 % [1]. The fast-growing demand use of asphalt mixture causes more pressure on the natural aggregate resources. In addition, asphalt pavement is vulnerable during service life due to being directly subjected to the environment and bearing traffic loads. Therefore, an improvement in asphalt mixture performance not only prolongs the service life but also reduces the pressure on natural resources. Nowadays, a lot of studies have been conducted to improve the properties of asphalt mixture. For instance, the utilization of coated fiber to enhance mechanical properties [2], using phase change material to mitigate the negative effect of environmental temperature [3,4]. Several studies aimed to prolong the service life of asphalt pavement by using induction or microwave heating to heal micro-cracks in the asphalt mixture [5,6], and using grid reinforcement to lessen the negative effect of reflection cracking [7,8]. Nevertheless, prolonging pavement service life is considered as an effective solution due to the environmental and cost-effectiveness.

Reflection cracking is one of the most common distresses that deteriorate asphalt pavement properties. Reflection cracking damages the structural strength of the pavement system from the bottom to the surface. Once it happens, the permeable property of pavement is increased, thus water easily penetrates, resulting in deterioration of pavement structure [9]. Based on the propagation of reflection cracking, several methods have been developed to prevent it, consisting of paving a thin layer at the interface between old and new pavement [10], using a special asphalt concrete [11]. However, utilizing grid is considered an effective method [12–14]. For past decades, grid reinforcement in asphalt pavement has been widely used such as roadways, railroads, and airports [15]. Especially, using grid in the flexible pavement is a hot topic that attracts many researchers. The grid presence in asphalt pavement has an essential effect during crack propagation. The grid also has been effective in reducing permanent deformation and distributing traffic loads with pavement foundation layers [16–18]. The Gonzalez-Torre's study reported that fiber grid presented the best cracking resistance. In addition, the reinforced carbon fiber grid could improve cyclic as well as monotonic loading [19]. Besides grid types, the interlayer system plays an important role that affects the adhesive of the top and the bottom layer. The interface bond could affect the stress and strain of

* Corresponding author.
E-mail addresses: yummy0220@induk.ac.kr (S.-Y. Lee), dpark@kunsan.ac.kr (D.-W. Park).

https://doi.org/10.1016/j.conbuildmat.2022.128954
Received 18 April 2022; Received in revised form 14 August 2022; Accepted 21 August 2022
Available online 29 August 2022

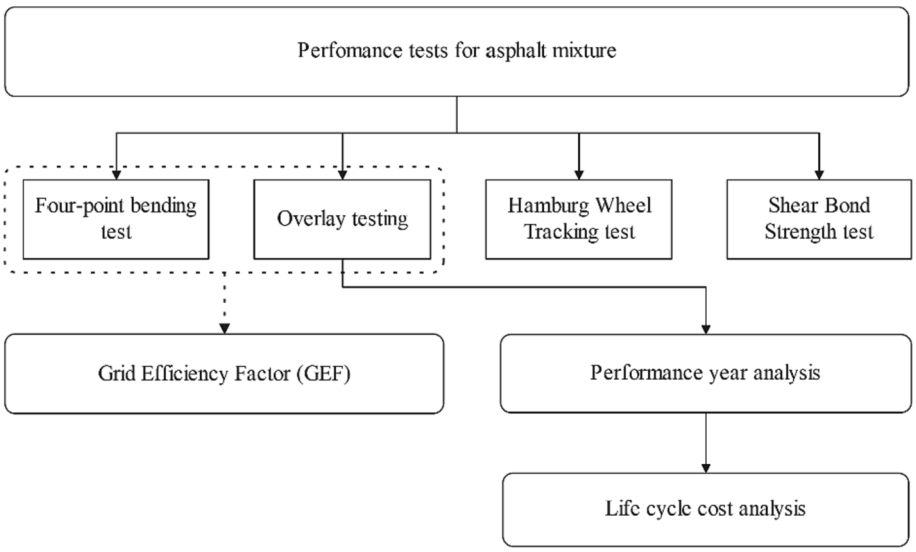

Fig. 1. Research flowchart.

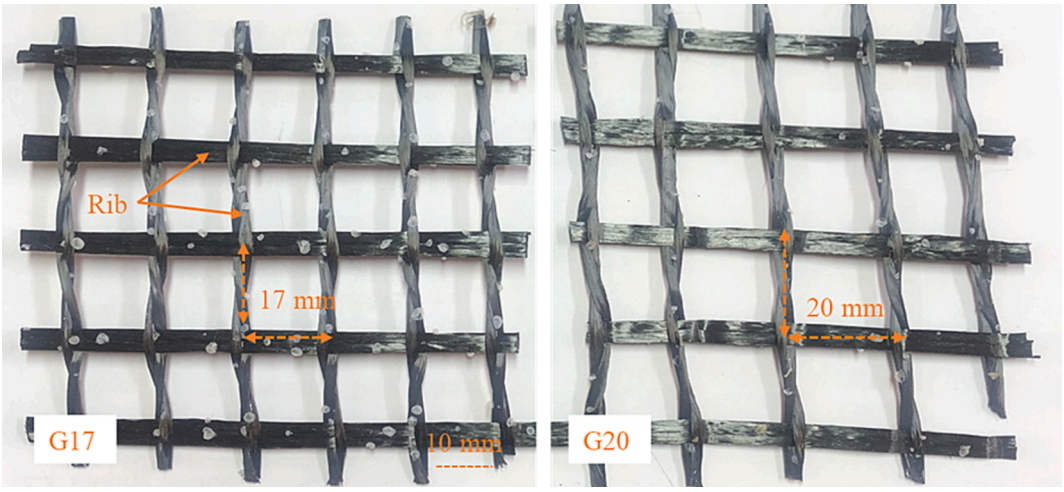

Fig. 2. G17 grid and G20 grid.

Table 1
Size gradation of aggregate.

Sieve size (mm)	19	12.5	9.5	4.75	2.36	0.6	0.3	0.15	0.075
Percent passing (%)	100	98	86	60	45	23	14	8	3

Table 2
Mixture configurations.

Description	Thickness	Mixture		
		C00	G17	G20
Top layer	30 mm	AC-13	AC-13	AC-13
Grid	1 mm	No	G17-grid	G20-grid
Tack coat	N/A	Yes	Yes	Yes
Bottom layer	30 mm	AC-13	AC-13	AC-13

the pavement structure. Several studies have proved that the adhesive strength of two layers should be adequate to ensure the proper working of pavement structure [7,20,21]. The research from Walubita et al. recommended shear bond strength should be higher than 225 kPa [7].

Besides research on the improved performances of geogrid, Zofka et al. recommended a procedure to quantify the benefit of grid on the service life of asphalt pavement. This procedure was developed based on an empirical and mechanical method [19]. The empirical-mechanical model could estimate the performance year of asphalt pavement based on the input of traffic, weather conditions, and asphalt geogrid pavement. Furthermore, the estimation of the performance year may be beneficial for the decision of maintenance or reconstruction of asphalt pavement. Life cycle cost analysis (LCCA) was firstly introduced by the American Association of State Highway and Transportation Officials (AASHTO) in 1986. Afterward, Life Cycle Cost Analysis software named RealCost has been developed by the Federal Highway Administration [22]. In the LCCA process, the cost efficiency of alternatives was determined based on Net Present Value (NPV). The analysis from LCCA could help highway agencies to decide on pavement rehabilitation strategies.

The current research aims to analyze the advantages of grid

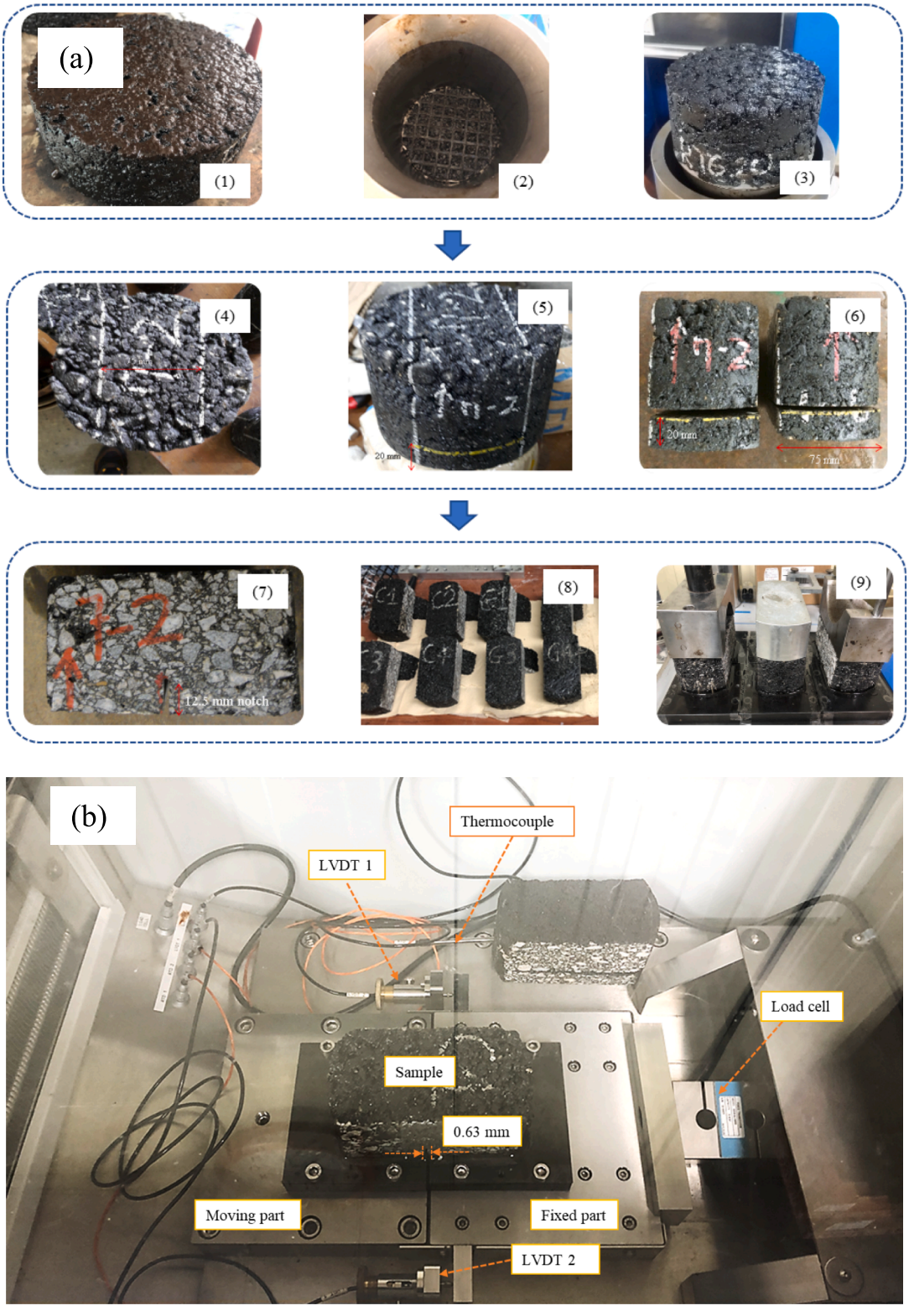

Fig. 3. OT sample preparation process (a) and OT test set up (b).

reinforcement on the performance properties as well as cost benefits of asphalt mixtures. In addition, two types of carbon grids, named G17 and G20 were considered, to evaluate the effect of grid characteristics. Several laboratory performance tests were conducted. Fatigue cracking and reflection cracking resistance were evaluated using the four-point bending test and OT test. Hamburg wheel tracking test was employed to determine the rutting resistance of grid reinforced mixtures. The adhesive strength between two layers of asphalt mixture was examined by a shear bond strength test. The effect of grid improvement on cracking resistance was computed by grid efficiency factor (GEF). The results of the OT test were utilized to analyze the pavement performance year of different asphalt mixtures through an empirical-mechanical reflective cracking model. Finally, a life cycle cost analysis of three different asphalt mixtures was conducted based on the outcomes from

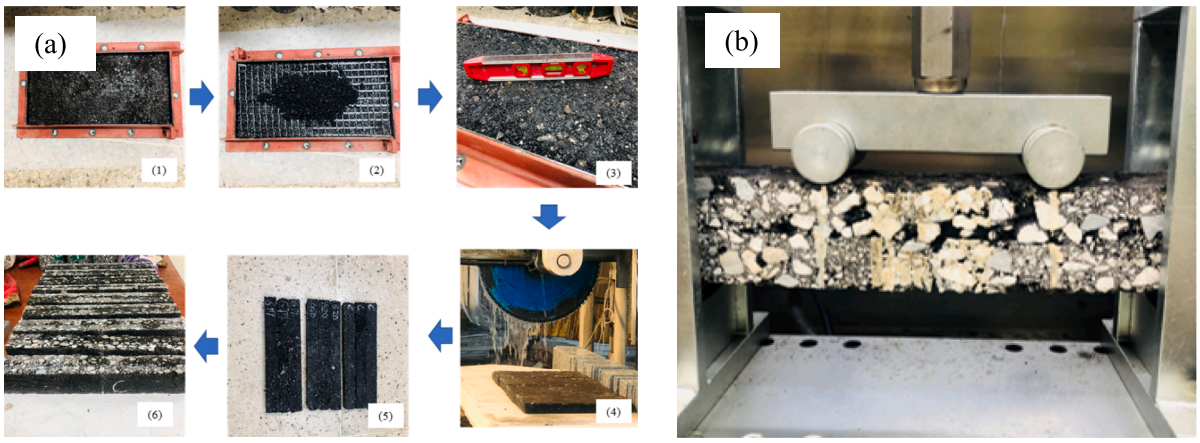

Fig. 4. Preparation of beam sample (a) and test set up (b).

Table 3
Four-point bending test specifications.

Item	Specification
Loading mode	Load-controlled
Input load magnitude (P_{max})	0.70 kN
Contact sitting load	0.035 kN (5 % of P_{max})
HMA beam sample dimensions	380 mm × 50 mm × 50 mm
HMA beam notch at the bottom	5 mm in depth, 3 mm in width
Target AV	7 ± 1 %
HMA beam sample replicates	≥3
Test termination	20 mm or 10,000 cycles

the pavement performance year analysis. The research flowchart is displayed in Fig. 1.

2. Materials

Two carbon grids were considered in this study, named G17 and G20. As shown in Fig. 2, both grids present a bare structure. The G17 and G20 grid form a square aperture with a size of 17 mm and 20 mm, respectively. Rib thickness ranged from 0.3 to 0.5 mm at the junction. The tensile modulus and tensile force of the grid were 73 GPa and 120 kN/m, respectively.

Dense grade hot mix asphalt with the nominal maximum aggregate size of 13 mm was used to fabricate samples. Aggregate size gradation is shown in Table 1. The PG 64-22 asphalt binder was used in this study. The binder has a penetration of 70 (25 °C, 0.1 mm), a melting point of 48 °C, and a density of 1.02 g/cm^3. The presence of grid layer could reduce the interface shear strength between two layers. Therefore, a modified asphalt emulsion tack coat, named BD tack coat was used to ensure adhesion between layers [23]. The polymer-modified tack coat has ductility, and penetration of 100 cm and 60 °C, respectively. For each mixture at least three samples were prepared. Mixture configurations are displayed in Table 2.

3. Test - analysis methods

3.1. Performance tests

3.1.1. OT test

The overlay tester (OT) test provides an excellent correlation to the propagation of reflection cracking. Fig. 3 illustrates the sample preparation process. Hot mix asphalt 13 mm was used to prepare samples. The bottom layer having a size of 150 mm in diameter and 50 mm in height was firstly compacted with the air void of 7 ± 1 %. Then, this layer was stabilized at room condition for 24 h before applying the tack coat layer. In this study, a polymer-modified tack coat was applied on the top of the bottom layer with a dosage of 0.45 litter/m^2. To dry the tack coat layer, sample was conditioned at ambient temperature for at least 4 h before applying grid. The sample was delivered to a 150 mm cylindrical mold

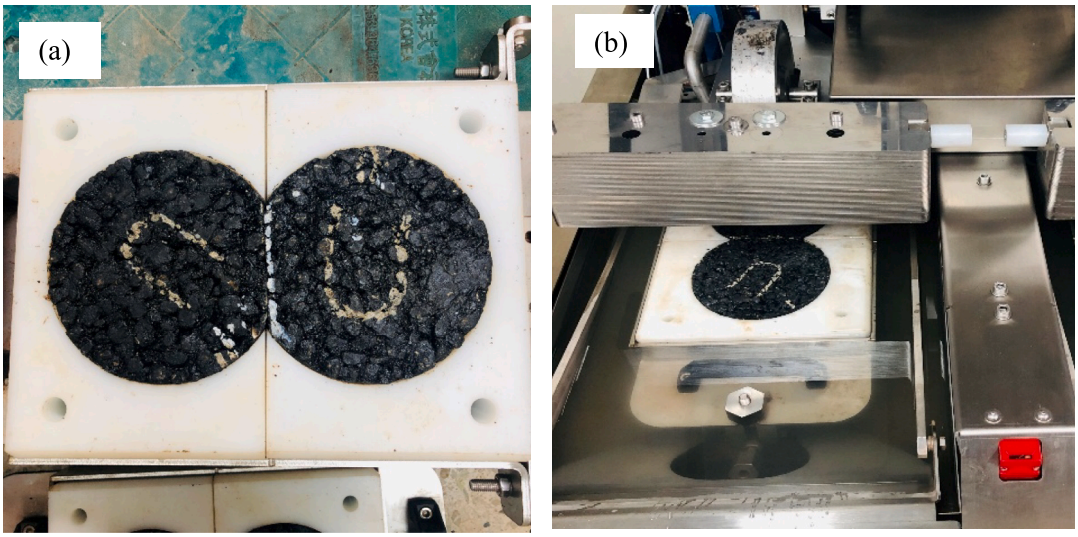

Fig. 5. Preparation of HWTT sample and (b) HWTT test set up.

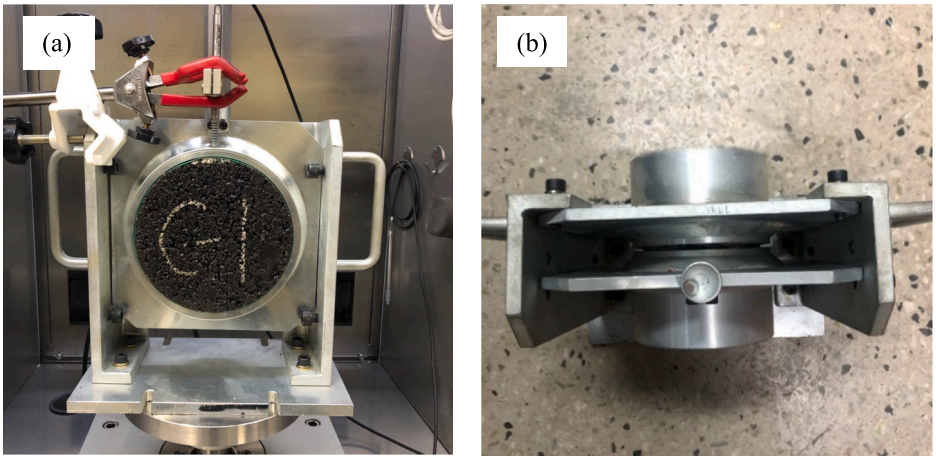

Fig. 6. Shear-bond test set up front view (a) and top view (b).

Table 4
Summary of input data for pavement performance year analysis.

Asphalt overlay information		Input data
Type		AC/PCC
RCR termination criteria		50 %
Traffic data	ADT	50,000 per day
	Operation speed	80 kph
	Climate data (10-year period)	From −5 °C to 38 °C
HMA overlay	Thickness	50 mm
	Mix type	Dense grade, PG 64-22
	Load cycles	From OT test
	Coefficient of thermal expansion	2.43×10^{-6} mm/°C
	Dynamic modulus	Following AASHTO T324
	Poisson ratio's	0.35
PCC layer	Thickness	200 mm
	Mix type	JPCP
	Coefficient of thermal expansion	9.9×10^{-6} mm/°C
	Poisson ratio's	0.15
	Modulus	27,560 MPa
	Load transfer efficiency	50 %
Base layer	Thickness	200 mm
	Type	Granular base
	Poisson ratio's	0.35
	Typical modulus	1035 MPa
Subgrade	Poisson ratio's	0.4
	Typical modulus	70 MPa

Table 5
1-km cost for single operation (Million Korean Won).

Solution	C00	G17	G20
Construction	179	288	258
Maintenance	51	86	77

to compact the top layer. The final height of the sample was controlled at 80 ± 1 mm including grid layer. The top and direction of compaction were also marked in white coloring and red (after cutting) so as to keep track of the top and bottom of the samples. White lines were marked at 75 mm apart in the middle zone of the molded samples to define the cutting width of the final OT specimens. Only the bottom side of the samples was trimmed at 20 mm to ensure a smooth surface for gluing to the OT plates. All the samples were notched to 12.5 mm depth from the bottom to simulate existing cracks on an existing pavement structure. After notching, samples were dried in room condition for 48 h before gluing on OT plates. In order to glue the sample to the OT plate, the high-strength 2-part epoxy (14 ± 2 g) was used. The epoxy was allowed to set and cure for a minimum period of 12 h with a 4.5 kg curing weight at room temperature (i.e., 25 °C).

In this study, the overlay test was performed based on the test procedure Tex-248-F [24]. The OT test was conducted with a testing temperature of 25 ± 1 °C. Glued samples were conditioned in a temperature incubator for three hours before testing. This test was conducted under control-strain mode with a maximum opening displacement of 0.63 mm as shown in Fig. 3b. One OT cycle consists of 5 s of opening and 5 s of closing. The test was terminated at 83 % of reduction peak load or reaching 1200 cycles, whichever is first. Each mixture was tested with four samples for average. Load versus the number of OT cycles were recorded during OT test. In general, a mixture with a higher OT cycle indicated a better cracking resistance.

In addition, the result of different grid reinforced mixtures was compared by Tukey-Kramer (T-K) Post Hoc test. To perform T-K analysis, one-way ANOVA (Analysis of Variance) was firstly used to determine whether or not there is a statistically significant difference between mixtures. Then, the T-K was employed to find which mixtures are different from each other [2]. In the current study, the T-K test was completed in Python programming language using available packages, named SciPy and StatsModels [25].

3.1.2. *Four-point bending test*

The four-point bending test aims to analyze the fatigue cracking resistance of asphalt mixture under repeated load. The air void of the beam sample was 7 ± 1 %. To achieve the target air void, the weight of the mixture was controlled by the sample's volume and density of the slab sample. As shown in Fig. 4a, a slab mold has a dimension of 250 mm in width, 500 mm in length, and 50 mm in thickness. The bottom layer was firstly compacted with a height of 25 mm using a hand compactor. This layer was conditioned at room temperature for 24 h before applying the tack-coat layer. The tack-coat layer was brushed on the surface with a content of 0.45 L/m^2. After drying for three hours, a grid layer, which has a size of 250 × 500 mm was applied to the tack-coat layer. Then, the asphalt mixture was filled in the mold and compacted to reach 50 mm height. The slab sample was conditioned for 24 h prior to cutting. A slab sample was cut into three beam samples. The final size of the beam sample was 50 mm in width, 50 mm in wide, and 380 mm in length. To emulate cracking, a notch having 3 mm wide and 5 mm depth, was firstly applied from front to back of the sample at the middle of the beam sample. Finally, beam samples were let dry for 72 h before testing.

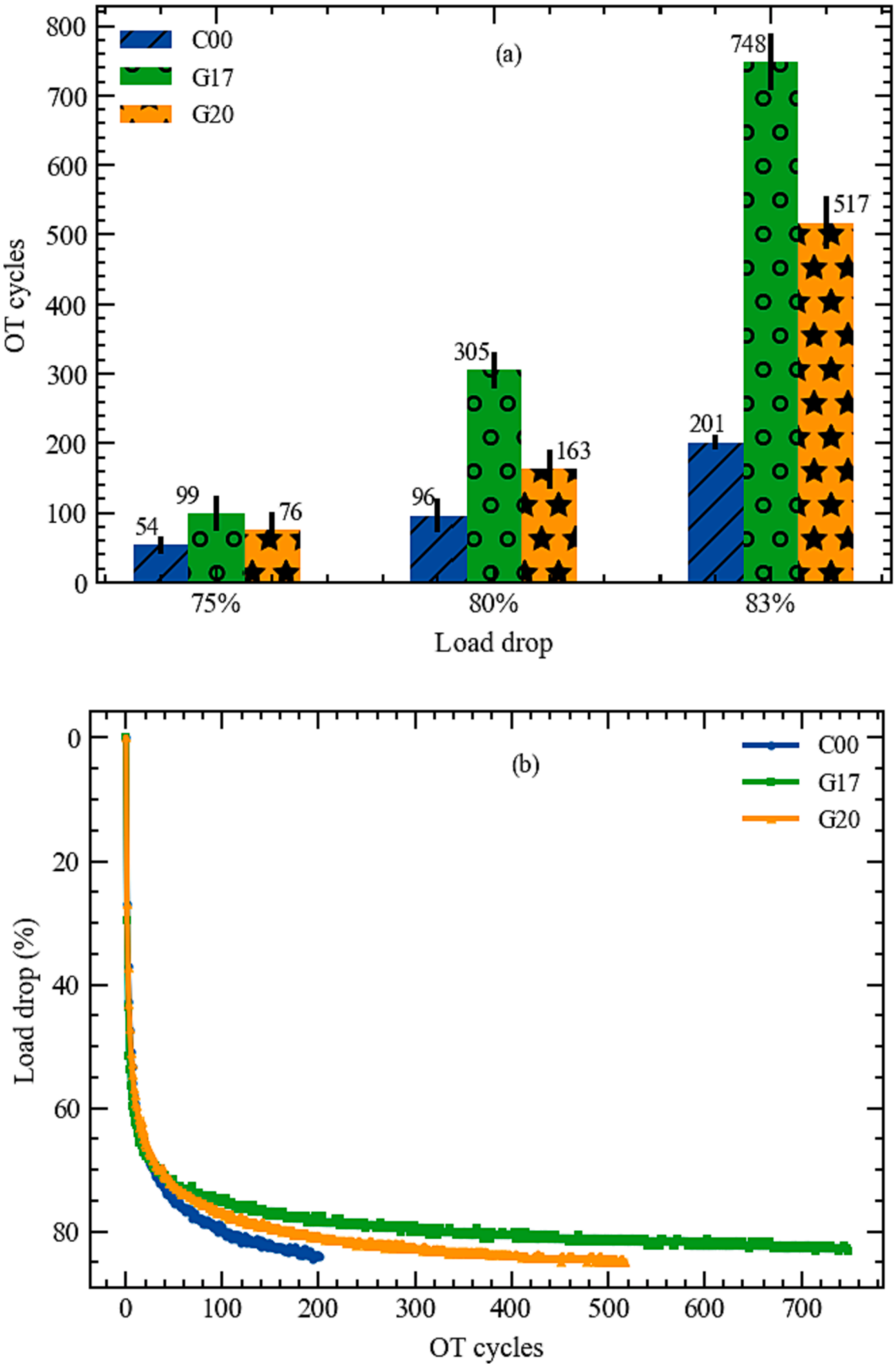

Fig. 7. OT cycles (a) and OT cycles-load drop (b).

Table 6
Tukey-Kramer multiple comparison (studentized q = 0.05).

group1	group2	Diff	Lower	Upper	p-value	Conclusion
C00	G17	547.3	385.4	709.2	0.001	Significantly different
C00	G20	316.7	154.8	478.6	0.002	Significantly different
G17	G20	230.7	68.8	392.6	0.011	Significantly different

To reach the equivalent temperature distribution, beam samples were conditioned in a temperature incubator at 20 ± 1 °C for three hours. The test is conducted based on AASHTO T 321 under control stress mode [26]. The test setup is shown in Fig. 4b. The loading waveform was a haversine load with a magnitude of 0.7 kN and a frequency of 5 Hz. The contact sitting load was 0.035 kN. The specification of the four-point bending test is shown in Table 3. This test was terminated at complete crack failure or 10,000 loading cycles, whichever is first. Finally, the Turkey-Kramer statistical analysis was employed to find the difference between mixtures in terms of the loading cycle.

3.1.3. Hamburg wheel tracking test

Hamburg wheel tracking (HWTT) test provides an evaluation of the moisture effect as well as rutting resistance of asphalt mixture. The sample preparation process of the HWTT test was similar to the process of the OT test. Samples were compacted by Superpave Gyration Compactor with the target air void of 7 ± 1 %. Based on the AASHTO T324-11 [27], the cylindrical sample was cut along a secant line such that when joined together in the molds there is no space between the cut edges as shown in Fig. 5a. After cutting, samples were conditioned at room temperature for 48 h before testing. Three samples were prepared for each mixture. In the current study, the test was conducted under the submerged condition as shown in Fig. 5b. The testing temperature was controlled at 50 ± 1 °C. The Hamburg Wheel Tracking load was 705 ± 5 N. A 203 mm steel wheel made 52 ± 2 passes across the specimen per minute, at approximately 0.305 m/s. The number of wheel passes and rut depth were recorded during the test. This test was terminated when the number of passes reach 20,000 or rut depth is 12.5 mm, whichever is first. Finally, the *T*-K statistical analysis was employed to find the difference between mixtures in terms of the HWT cycle.

3.1.4. Shear bond strength test

Shear bond strength test is used to evaluate the bonding strength of two layers. This test applies a constant shear displacement rate across the interface of two layers. This test was performed on the 150 mm two-layer sample. The sample preparation process was similar to the OT process; however, the final height of the sample was 100 mm, which is 50 mm for each layer. Three samples were prepared for each mixture. The samples were conditioned in a temperature incubator at 20 ± 1 °C for three hours prior to testing. Based on TEX-249-F, the shear bond strength test was adopted with a loading rate of 5 mm/min at 20 ± 1 °C [23]. The sample was covered by tape to prevent sticking to the jig. The interlayer should be in the middle of the jig. The test setup is shown in Fig. 6. During the test, load displacement was recorded. The shear bond strength was calculated by equation (1). Finally, the Turkey-Kramer statistical analysis was employed to find the difference between mixtures in terms of shear bond strength.

$$S_{\max} = \frac{4P_{\max}}{\pi D^2} \tag{1}$$

where

S_{max}: shear bond strength (MPa),
P_{max}: maximum load (kN),
D: diameter of sample (mm).

3.2. Grid efficiency factor

The grid efficiency factor (GEF) is used to compare the relative performance of grid reinforced mixture and conventional mixture without grid. The grid efficiency factor is developed based on the idea of traffic benefit ratio (TBR), which followed the AASHTO R 50-09 [28]. The TBR is calculated by the ratio of the number of load cycles a reinforced pavement structure required to reach a defined failure state to the number of loads the same unreinforced section required to reach the same defined failure state [28]. The traffic benefit ratio calculation is displayed in Eq. (2).

$$TBR = \frac{N_{grid}}{N_{control}} \tag{2}$$

where

TBR: traffic benefit ratio,
N_{grid}: number of cycles to reach failure condition of grid reinforced mixture,
$N_{control}$: number of cycles to reach failure condition of control mixture.

In this study, two grid efficiency factors were determined based on the result of the overlay test and four-point bending test. The defined failure state was 83 % load drop and 10 mm deformation for the OT test and four-point bending test, respectively. The GEF is calculated by the following Eq. (3). Because the OT test and four-point bending test were conducted on the laboratory samples, the lab-fired shift factor was used to reflect the behavior of the mixture under field conditions. Based on the recommendation from Walubita's research, the SFIR of 0.41 was selected [29].

$$GEF = TBR \times SF_{IR} \tag{3}$$

where

TBR: traffic benefit ratio,
SF_{ir}: lab-fired shift factor from the literature.

3.3. Life cycle cost analysis

3.3.1. Performance year based on OT cycles

Reflective cracking rate (RCR) is one of the most important factors to consider when designing the thickness of the HMA overlay. The mechanical empirical reflective cracking rate (ME-RCR) prediction algorithm was introduced in the Zhou and Hu studies [30–33]. Following these research, an Excel VBA program was developed to predict the reflective cracking rate as well as predict the performance year of asphalt overlay on plain cement concrete (AC/PCC) [8]. The daily crack propagation (ΔC) is shown in Eq. (4).

$$\Delta C = k_1(K_b)^n \Delta N + k_2 A(K_s)^n + k_3 A(K_{th})^n \tag{4}$$

where

ΔC: daily crack length increasement,
ΔN: daily load repetitions,
K_b, K_s, K_{th}: stress intensity factor (SIF) caused by bending, shearing, and thermal loading, respectively,
k_1, k_2, k_3: calibration factors.

A and *n* parameters are fracture properties obtained from the power regression curve defining the relationship of crack length per OT cycle. Zhou et al, recommended the calculation of two parameters in Eq. (5) [32].

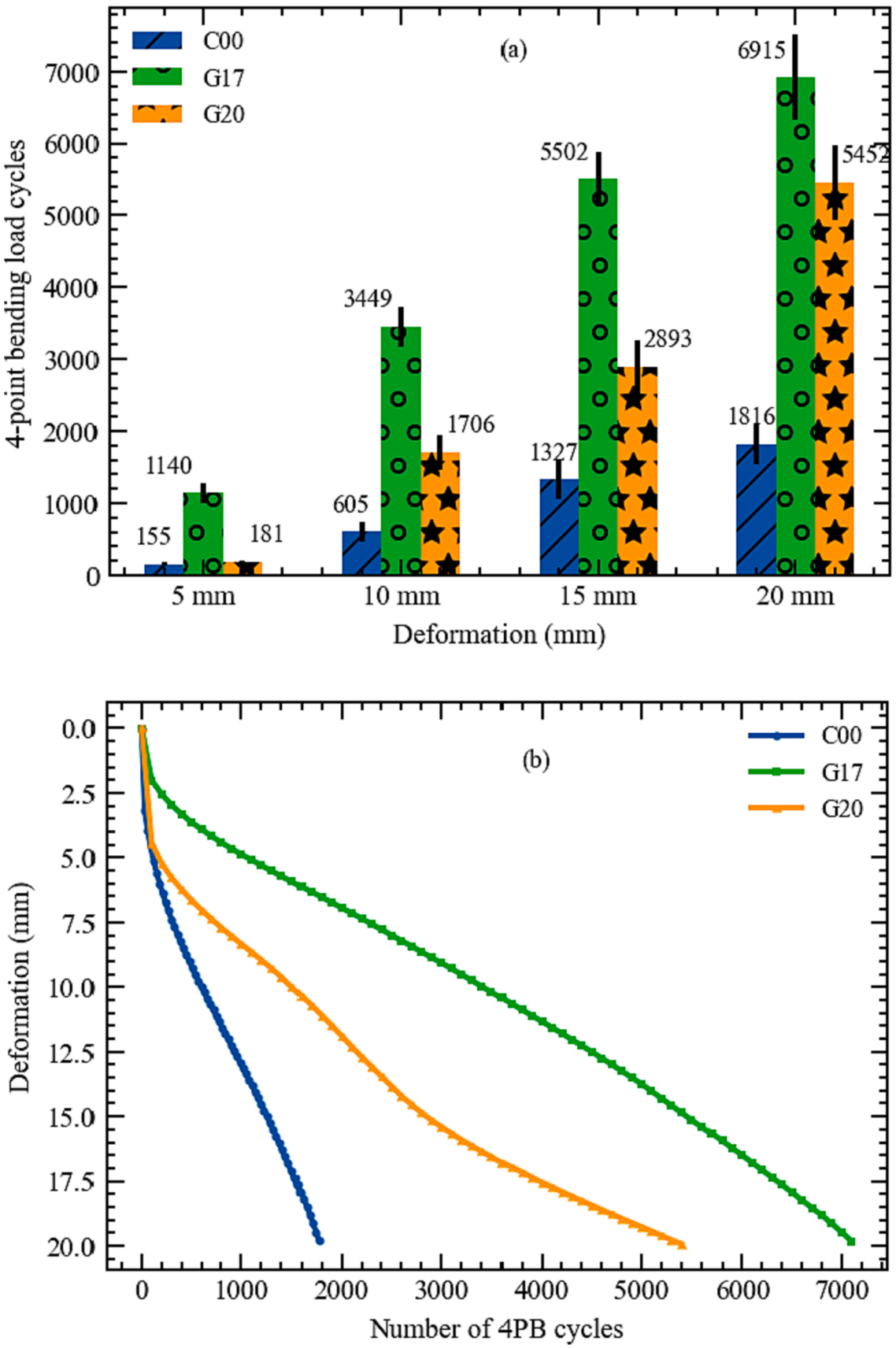

Fig. 8. Loading cycles (a) and load cycle-deformation (b).

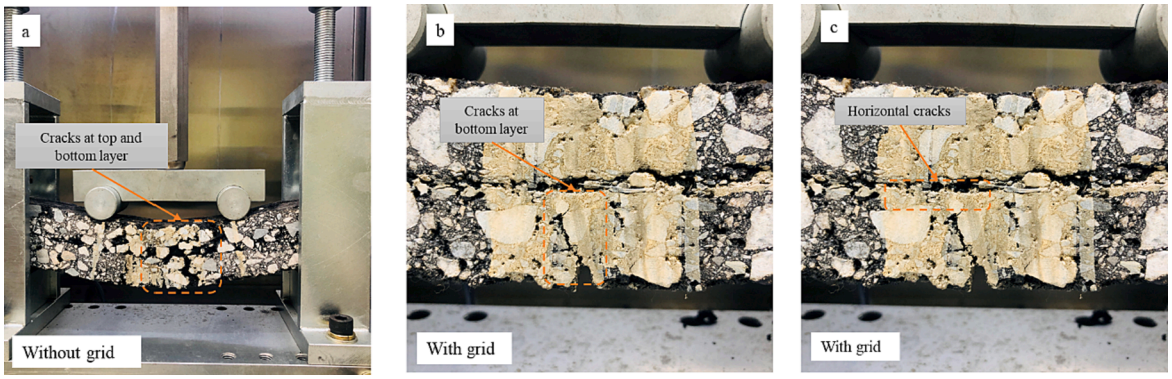

Fig. 9. Cracks in beam sample without grid reinforcement (a) and with grid reinforcement (b, c).

Table 7
Tukey-Kramer multiple comparison (studentized q = 0.05).

group1	group2	Diff	Lower	Upper	p-value	Conclusion
C00	G17	5098.6	3968.5	6228.1	0.001	Significantly different
C00	G20	3638.7	2508.9	4768.5	0.001	Significantly different
G17	G20	1549.7	329.9	2589.5	0.017	Significantly different

$$A = 0.0044(n_{OT})^{-1.91}$$

$$n = 0.524\ln(n_{OT}) + 2.047 \quad (5)$$

where

n_{OT}: number of OT cycles obtained from the OT test.

Finally, the reflection cracking rate was computed in an empirical sigmoidal function as shown in Eq. (6).

$$RCR = \frac{100}{1 + e^{C_1 \log\left(\frac{\Delta C}{H_0}\right)}} \quad (6)$$

where

RCR: reflective cracking rate,
C_1: relationship between fatigue distress versus damage,
H_0: is HMA overlay thickness.

The analysis of pavement performance year requires the input data, consisting of climate data, traffic, material properties, and the number of OT cycles. The summary of input data is shown in Table 4. The main objective is to calculate the performance year of asphalt overlay with grid reinforcement. In the previous study, the performance year was defined as the duration of acceptable service life wherein the RCR was less than 50 % [8]. The performance years from this analysis were utilized to select alternatives in the life cycle cost analysis.

3.3.2. Life cycle cost analysis

In this study, the Excel VBA Program named RealCost 2.5 was used to analyze the life cycle cost [22]. It is a program developed by Federal Highway Administration (FHWA) based on Microsoft Excel with Visual Basic for Application code. The main result from RealCost was NPV (Net Present Value), which represented the economic efficiency indicator of the alternative. The NPV is calculated using the following Eq. (7).

$$NPV = \sum_{k=1}^{N} (AC + OC)_k \frac{1}{(1+i)^k} \quad (7)$$

where

NPV: net present value,
AC: Agency Cost,
OC: Operation cost,
i: discount rate (%),
N: year of expenditure,
k: is estimated for year k^{th}.

Three alternatives are considered to analyze the life cycle cost, including C00, G17, and G20 corresponding to dense grade asphalt mixture without grid reinforcement, dense grade asphalt mixture with G17 grid, and dense grade asphalt mixture with G20 grid. In order to decide on construction or maintenance alternatives, the outcomes from the performance year analysis were considered. Construction cost and maintenance cost for a single operation is shown in Table 5. Finally, the salvaged cost was ignored in this analysis.

4. Results and discussion

4.1. Performance tests

4.1.1. Overlay test

The result of the OT test under cyclic fatigue loading is displayed in Fig. 7a. Overall, reinforced grid mixtures gained a higher number of OT cycles than that without grid reinforcement. The G17 mixture acquired the highest OT cycle among the three mixtures. At 83 % load drop, G17 gained 748 cycles while that of the control mixture and the G20 mixture were 201 and 517 cycles, respectively. Using G17 grid reinforcement increases the number of OT cycles by more than four times compared to a conventional mixture.

In addition, the relationship between the number of OT cycles and load drop is shown in Fig. 7b. Grid reinforced asphalt mixture presented a lower reduction in load drop than that of the control mixture. This phenomenon can be explained by the grid layer potentially disappearing as a part of reflection cracking. The grid at the interlayer could mitigate crack propagation from the bottom to the top of the sample, thus resulting in a decrease in the load drop of the sample. Tukey-Kramer analysis was employed to consider the difference between mixtures in terms of the number of OT cycles. As shown in Table 6, the p-values of the three comparisons were less than 0.05, which confirmed that there was a significant difference between grid mixtures and the control mixture. In other words, the grid reinforcement could increase resistance to reflection cracking of asphalt mixture.

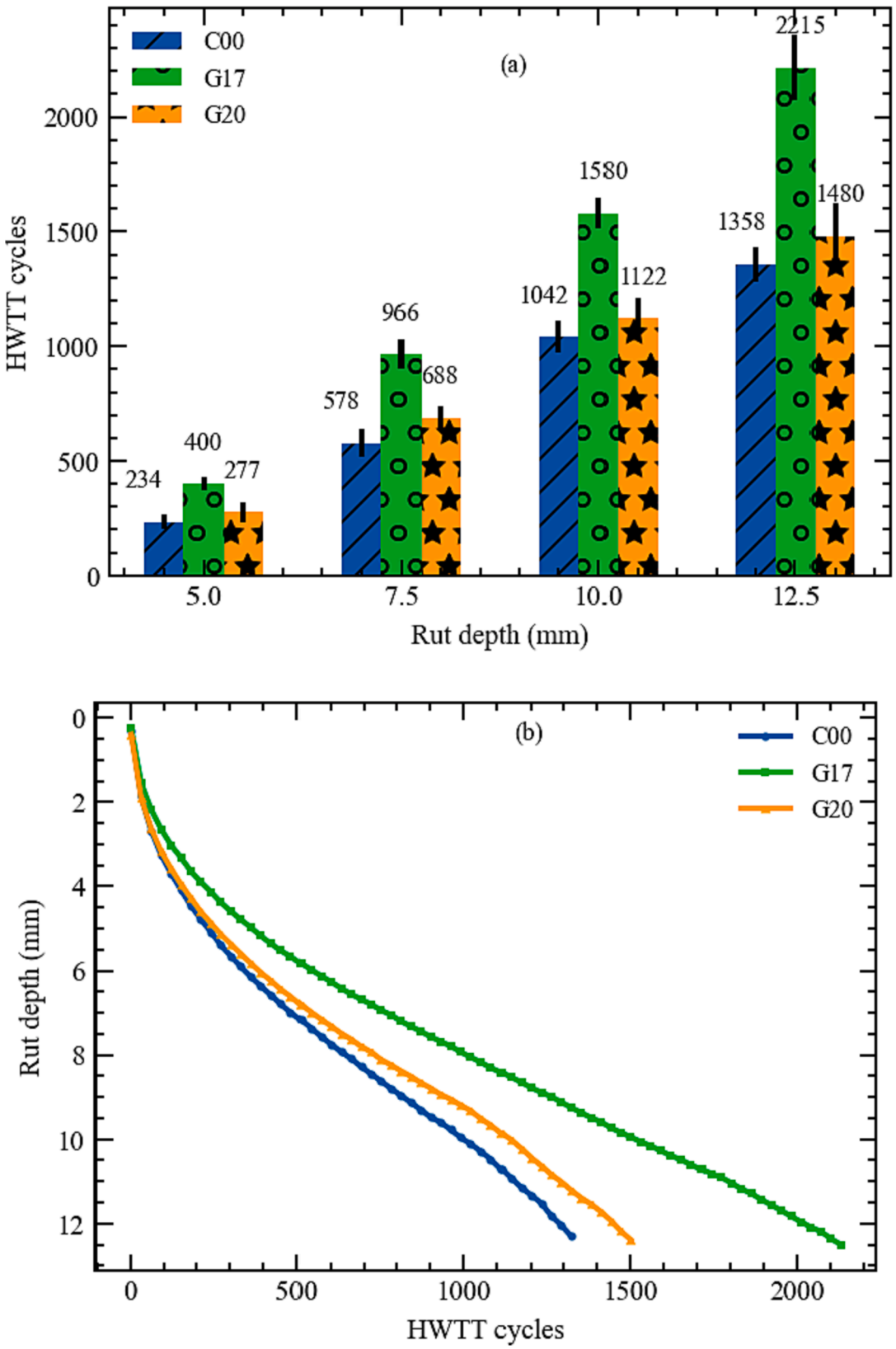

Fig. 10. Hamburg wheel tracking result (a) and relationship between rut depth and HWTT cycles (b).

4.1.2. Four points bending test

Fig. 8 displays the number of loading cycles of three asphalt mixtures. In general, mixtures with grid gained higher loading cycles than conventional mixtures at the same level of deformation. For example, the loading cycles of the C00, G17, and G20 mixture were 605, 3449, and 1706 cycles at 10 mm deformation, respectively. The deformation-loading cycle behavior of mixtures in this test was similar to the result from the OT test. The grid reinforced mixtures presented a lower

Table 8
Tukey-Kramer multiple comparison (studentized q = 0.05).

group1	group2	Diff	Lower	Upper	p-value	Conclusion
C00	G17	856.3	236.6	1476.1	0.013	Significantly different
C00	G20	122.0	−497.7	741.7	0.81	Not significantly different
G17	G20	734.3	114.6	1354.1	0.025	Significantly different

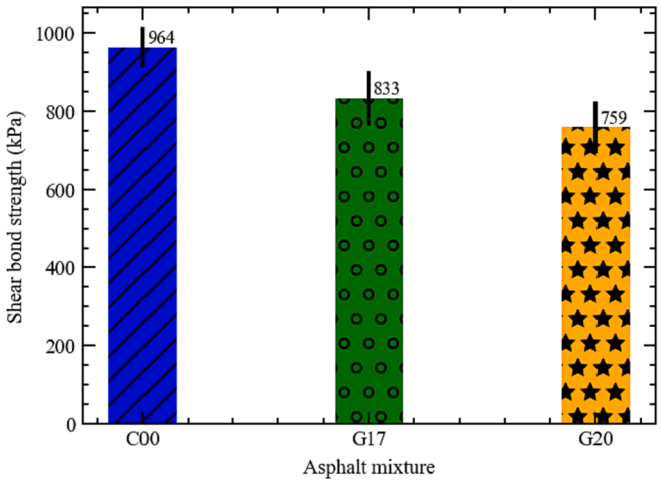

Fig. 11. Shear bond strength.

Table 9
Tukey-Kramer multiple comparison (studentized q = 0.05).

group1	group2	Diff	Lower	Upper	p-value	Conclusion
C00	G17	128.3	11.3	245.4	0.035	Significantly different
C00	G20	202.3	85.3	319.4	0.004	Significantly different
G17	G20	74.0	−43.1	191.1	0.208	Not significantly different

deformation velocity that than of control mixture, which indicated better fatigue cracking resistance.

Regarding mixture without grid reinforcement, cracks propagated from the bottom to the top layer as shown in Fig. 9a. This phenomenon led to high deformation. In contrast, there were no cracks above the interlayer layer of grid reinforced mixtures. The cracks only existed at the bottom layer (Fig. 9b). This may be due to the grid layer being able to prevent crack propagation from the bottom. When the cracks propagated to the grid interlayer, a horizontal direction change in the crack propagation was observed as displayed in Fig. 9c. This is because the debonding is located between the top and bottom layers. The direction change in crack propagation may be beneficial in delaying the appearance of a reflective crack in the top layer [34]. In addition, the multiple comparisons from the *T*-K analysis showed that there was a significantly different between grid reinforced mixture and conventional mixture as displayed in Table 7.

4.1.3. Hamburg wheel tracking test

The number of Hamburg wheel tracking cycles at several rut depths is displayed in Fig. 10a. Overall, the grid reinforced mixtures gained an enhancement in rutting resistance compared to the control mixture. Especially, the G17 grid reinforced mixture presented the best resistance

Table 10
Data variability and statistical analysis.

Test	Mixture	Data	Average	Stdev.	COV (%)	T-K analysis
OT	C00	219; 205; 178	201	21	10.4	C00-G17 = YES
	G17	689; 715; 840	748	81	10.8	C00-G20 = YES
	G20	434; 539; 579	517	75	14.5	G17-G20 = YES
Four-point bending	C00	1,501; 1,994; 1,955	1,816	274	15.1	C00-G17 = YES
	G17	6,230; 7,002; 7,513	6,915	646	9.3	C00-G20 = YES
	G20	5,261; 5,855; 5,521	5,452	346	6.3	G17-G20 = YES
HWTT	C00	1,501; 1,373; 1,201	1,358	151	11.1	C00-G17 = YES
	G17	1,922; 2,232; 2,490	2,215	284	12.8	C00-G20 = NO
	G20	1,492; 1,758; 1,191	1,480	284	19.2	G17-G20 = YES
Shear bond strength	C00	983; 920; 981	964	36	3.7	C00-G17 = YES
	G17	836; 878; 784	833	47	5.7	C00-G20 = YES
	G20	698; 771; 807	759	56	7.3	G17-G20 = NO

to rutting among three asphalt mixtures. The G17 mixture acquired 2215 cycles compared to 1480 and 1358 that of G20 and C00 mixture, respectively. Noted that the samples in this test were two-layer samples and the height of each layer was 30 mm to meet the requirement of HWTT specifications. Therefore, the number of HWTT cycles could be lower than that of the single-layer sample [35].

In addition, the behavior of rut depth under HWTT load is illustrated in Fig. 10b. In general, grid reinforcement could delay the rutting velocity under repeated loading. The grid layer could alter a part of the applied vertical load to the horizontal direction during the loading process. Hence, the rutting effect could be mitigated. Table 8 indicated that there was a significant difference between G17 and other mixtures, meanwhile there was little differences between C00 and G20 mixture. It can be concluded that the reinforcement of the G17 grid could significantly improve the rutting resistance of the asphalt mixture.

4.1.4. Shear bond test

The shear bond strengths of asphalt mixtures are shown in Fig. 11. Overall, mixtures with a grid layer showed lower shear bond strength than that of the conventional mixture. The shear bond strength of the control mixture was 964 kPa compared to 833 and 759 kPa of the G17 and G20 mixture, respectively. The reinforced grid interlayer may reduce the contact area between two asphalt layers, thus resulting decrease in shear bond strength. However, both reinforced mixtures met the requirement of 225 kPa shear bond strength [7].

Considering shear bond strength of the G17 and G20 mixture, there was an insignificant difference between G17 and G20 in terms of shear bond strength. The reason may be due to both G17 and G20 grids consisting of the same material. In addition, statistical analysis was employed to compare the effect of grid layer on the shear bond strength. The result from Table 9 again confirmed that there was an insignificant

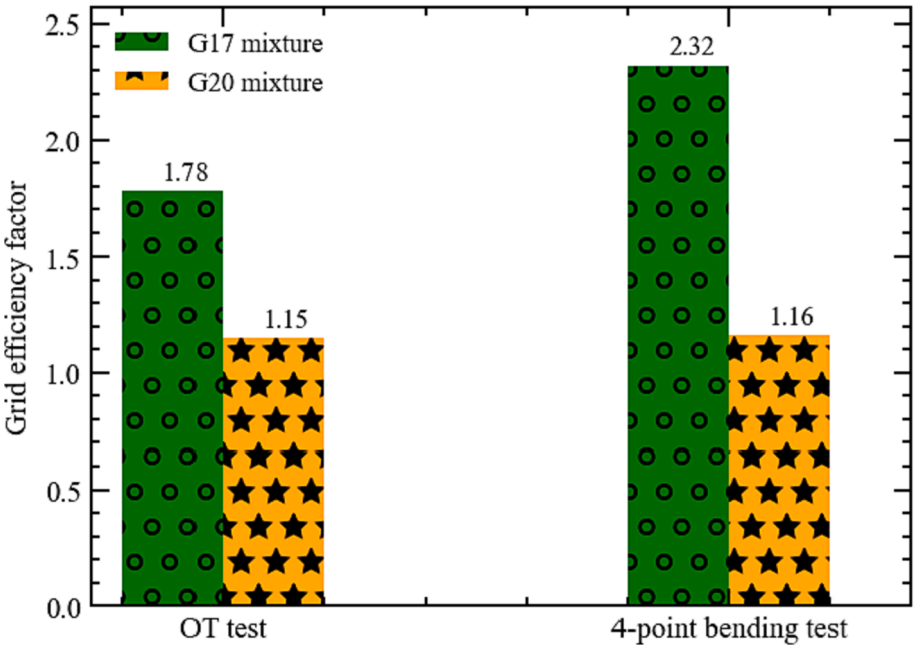

Fig. 12. Grid efficiency factor.

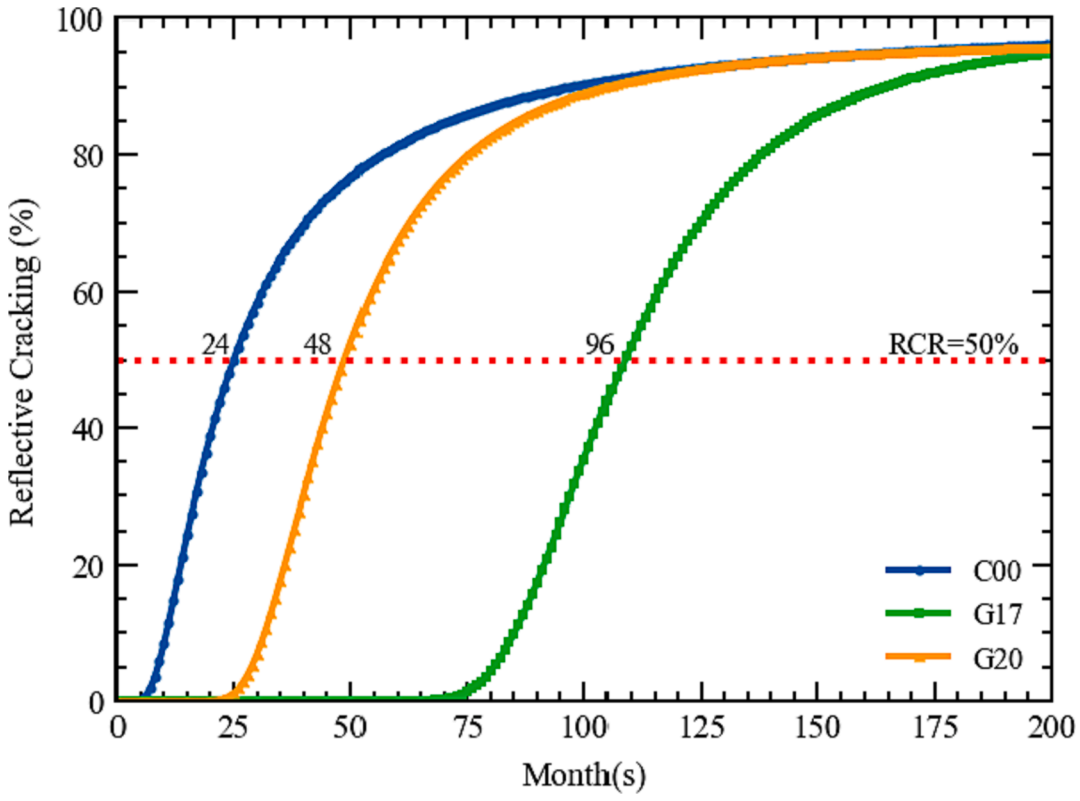

Fig. 13. Performance year analysis result.

Table 11
Construction and maintenance strategies through 20 years LCCA.

Year	0	2	4	6	8	10	12	14	16	18	20
C00	Δ	*	*	*	Δ	*	*	*	Δ	*	*
G17	Δ				*				*		
G20	Δ		*		*		*		Δ		*

Note: "*" is maintenance strategy; "Δ" is construction strategy.

difference between G17 and G20. Meanwhile, the shear bond strength of the control mixture was significantly different from the two grid reinforced mixtures.

4.1.5. *Test data quality and statistical variability*

Table 10 shows the data quality and statistical variability of performance tests. Overall, the collected data met COV (coefficient of variation) requirement [17]. Except for C00 and G20 mixture in Hamburg

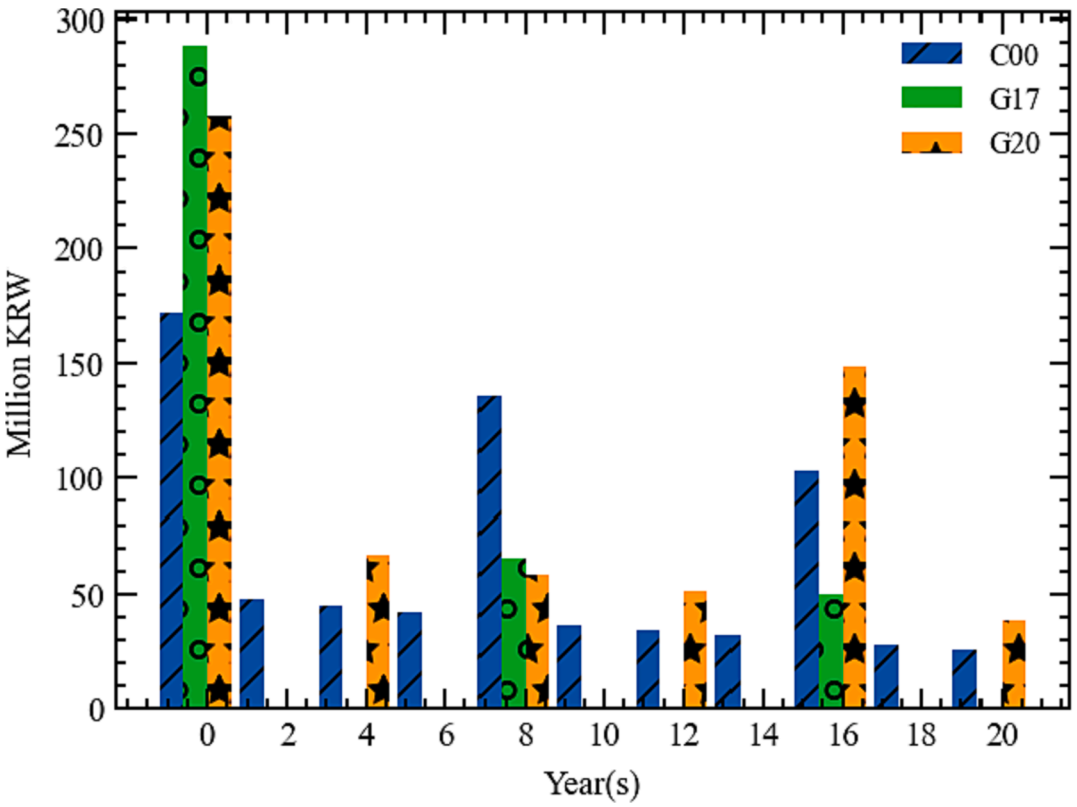

Fig. 14. Life cycle cost analysis (20 years).

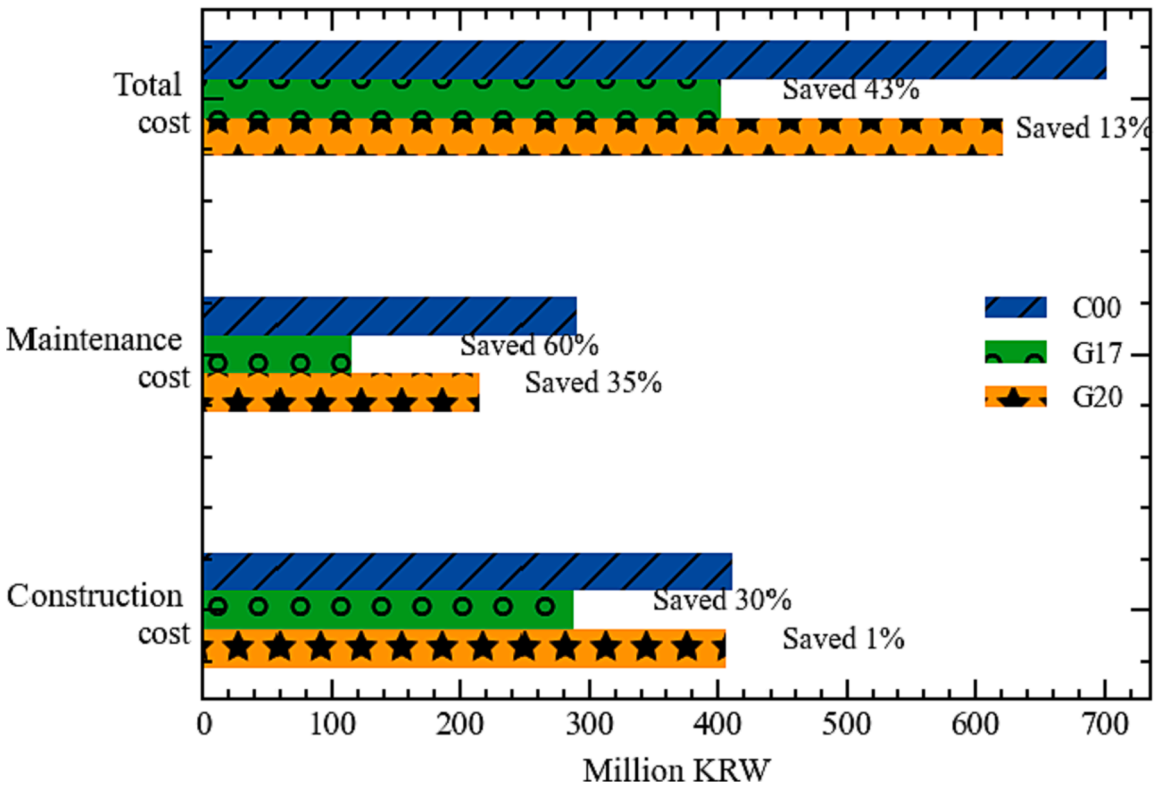

Fig. 15. Comparison between alternatives.

wheel tracking test, the Tukey-Kramer analysis indicated that all carbon grid reinforcement mixtures were statistically different from the control (without grid reinforcement). The insignificant difference between C00 and G20 in terms of HWTT can be traced to the standard error bar as shown in Fig. 10.

4.2. Grid efficiency factor

The results of grid efficiency factor are displayed in Fig. 12. The average number of cycles at the 83 % load drop of the OT test, and 10 mm deformation of the four-point bending test were selected to calculate grid efficiency factor. In general, the GEF of both mixtures was higher than 1.1, which implied an improvement in the performance of asphalt pavement. The GEF values from this study satisfied the requirement from the previous research, which was higher than 1.1 [36,37]. The grid efficiency factor of the G17 reinforced mixture outperformed G20 reinforced mixture, which was 1.78 compared to 1.15 in the OT test and 2.32 compared to 1.16 in the four-point bending test. The GEF value of 2.32 indicated that the G17 mixture can improve crack resistance by 2.32 times in service life [9]. The higher crack resistance may be beneficial in prolonging the service life.

4.3. Life cycle cost analysis

The performance year analysis of different grid reinforced asphalt mixtures is shown in Fig. 13. The performance year is defined as the duration of acceptable service life wherein the reflection cracking rate is less than 50 % [8]. From the analysis, the C00 mixture (201 OT cycles), G17 mixture (748 OT cycles), and G20 mixture (517 OT cycles) obtained a pavement performance year of 24 months, 48 months, and 96 months respectively. Overall, the grid reinforcement could increase the performance year of the asphalt mixture. This is because a grid could improve resistance to reflection cracking, which is displayed by the number of OT cycles. The outcomes from this analysis were consistent with the results from the performance test. The grid reinforcement could enhance the reflective cracking, thus prolonging the service life of asphalt pavement.

In addition, the outcomes from the performance year analysis were utilized to select construction and maintenance strategies. The alternative strategies designed for life cycle cost analysis are presented in Table 11. With the C00 alternative, maintenance is required every-two years to ensure a reflective cracking rate (RCR) of less than 50 %. This value for G17 and G20 alternatives is eight and four years respectively. Besides, after three maintenance works, the construction is conducted.

The life cycle cost analysis of the 20 years is shown in Fig. 14. Overall grid reinforcement required less maintenance and reconstruction than that of the control mixture. Therefore, the net present value of the two grid reinforced alternatives was extremely lower than that of the control alternative. Especially, the G17 alternative presented a 60 % saving in maintenance cost, and 30 % in construction cost compared to the control mixture, respectively. This is because the G17 alternative requires only two maintenances and zero reconstruction through 20-year service life. Meanwhile, the C00 alternative requires three reconstructions and eight maintenances. Finally, G17 and G20 acquired the lower total cost, which was 43 % and 13 % respectively (Fig. 15).

5. Conclusions

The current research aims to evaluate the advantages of grid reinforcement in asphalt mixtures. Two different grid types were considered, including G17 and G20. Asphalt mixture performances were examined by OT test, four-point bending test, Hamburg wheel tracking test, and shear bond strength test. In addition, the grid efficient factor was computed to reflect the improvement of grid reinforcement. The performance year of grid reinforced asphalt mixtures was estimated by the empirical-mechanical model. Then, the cost-benefit was analyzed by life cycle cost analysis. The following key findings can be drawn:

- Grid reinforcement mixtures exhibited a higher performance on fatigue cracking resistance. The OT cycles of the G17 reinforced mixture were approximately-four times than the mixture without grid.
- Using grid not only prevented cracks propagation to the top layer but also reduced deformation velocity. This is due to the transverse crack direction; grid reinforced mixture presented a better resistance to fatigue cracking.
- Carbon grid reinforced mixtures gained an enhancement in rutting resistance compared to the control mixture. Besides, grid interlayer could reduce shear bonding strength between two layers. However, both grid mixtures met the minimum shear bonding strength requirement of 225 kPa.
- The grid efficiency of the G17 mixture outperforms the G20 mixture, which was 2.5 compared to 1.16. The performance year of grid mixtures was 2–4 times than the control mixture.
- The economic efficiency conducted by LCCA showed that the G17 and G20 alternatives presented the best economical alternatives, which reduced 43 % and 13 % total cost respectively compared to C00 alternative through 20-year service.

In general, the current study provides an overview of carbon grid reinforced asphalt pavement. The addition of a carbon grid could improve the performance properties of asphalt pavement such as resistance to reflection cracking, reducing permanent deformation, and prolonging service life. It should be noted that more analysis (e.g., multiple testing temperatures) should be considered in further research.

CRediT authorship contribution statement

Sang-Yum Lee: Methodology, Validation, Data curation, Writing – review & editing, Writing – original draft. **Tam Minh Phan:** Data curation, Validation, Writing – original draft. **Dae-Wook Park:** Methodology, Validation, Data curation, Writing – review & editing.

Declaration of Competing Interest

The authors declare that they have no known competing financial interests or personal relationships that could have appeared to influence the work reported in this paper.

Data availability

Data will be made available on request.

Acknowledgment

This work was supported by the Korea Agency for Infrastructure Technology Advancement (KAIA) grant funded by the Ministry of Land, Infrastructure and Transport (Code **21RITD-C161698-01**). This study was also partially conducted under research project Development of High-Performance Concrete Pavement Maintenance Technology to Extend Roadway Life (Project No: **22POQW-B146690-05**) funded by KAIA.

References

[1] National Asphalt Pavement Assosiation, The Asphalt Pavement Industry Fast Facts, Natl. Asph. Pavement Assos. (n.d.). https://www.asphaltpavement.org.
[2] T.M. Phan, S.N. Nguyen, C.-B. Seo, D.-W. Park, Effect of treated fibers on performance of asphalt mixture, Constr. Build. Mater. 274 (2021) 122051, https://doi.org/10.1016/j.conbuildmat.2020.122051.
[3] B. Ma, S. Chen, Y. Ren, X. Zhou, The thermoregulation effect of microencapsulated phase-change materials in an asphalt mixture, Constr. Build. Mater. 231 (2020) 117186, https://doi.org/10.1016/j.conbuildmat.2019.117186.
[4] T. Minh Phan, D.-W. Park, T. Ho Minh Le, Improvement on rheological property of asphalt binder using synthesized micro-encapsulation phase change material, Constr. Build. Mater. 287 (2021) 123021. https://doi.org/10.1016/j.conbuildmat.2021.123021.
[5] J. Norambuena-Contreras, A. Garcia, Self-healing of asphalt mixture by microwave and induction heating, Mater. Des. 106 (2016) 404–414, https://doi.org/10.1016/j.matdes.2016.05.095.

[6] T.M. Phan, D.-W. Park, T.H.M. Le, Crack healing performance of hot mix asphalt containing steel slag by microwaves heating, Constr. Build. Mater. 180 (2018) 503–511, https://doi.org/10.1016/j.conbuildmat.2018.05.278.
[7] L.F. Walubita, X. Hu, T.P. Nyamuhokya, J.J. Komba, M. Souliman, Geogrid reinforcement in hot-mix asphalt: interlayer shear bond strength assessment, Transp. Res. Rec. (2018).
[8] A.B. Tam, D.-W. Park, T.H.M. Le, J.-S. Kim, Evaluation on fatigue cracking resistance of fiber grid reinforced asphalt concrete with reflection cracking rate computation, Constr. Build. Mater. 239 (2020) 117873, https://doi.org/10.1016/j.conbuildmat.2019.117873.
[9] H. Alimohammadi, J. Zheng, V.R. Schaefer, J. Siekmeier, R. Velasquez, Evaluation of geogrid reinforcement of flexible pavement performance: A review of large-scale laboratory studies, Transp. Geotech. 27 (2021) 100471, https://doi.org/10.1016/j.trgeo.2020.100471.
[10] I. Gonzalez-Torre, M.A. Calzada-Perez, A. Vega-Zamanillo, D. Castro-Fresno, Experimental study of the behaviour of different geosynthetics as anti-reflective cracking systems using a combined-load fatigue test, Geotext. Geomembr. 43 (2015) 345–350, https://doi.org/10.1016/j.geotexmem.2015.04.001.
[11] A. Wargo, S.A. Safavizadeh, Y.R. Kim, Comparing the performance of fiberglass grid with composite interlayer systems in asphalt concrete, Transp. Res. Rec. 2631 (2017) 123–132, https://doi.org/10.3141/2631-14.
[12] L.F. Walubita, A.N.M. Faruk, J. Zhang, X. Hu, Characterizing the cracking and fracture properties of geosynthetic interlayer reinforced HMA samples using the Overlay Tester (OT), Constr. Build. Mater. 93 (2015) 695–702, https://doi.org/10.1016/j.conbuildmat.2015.06.028.
[13] L.F. Walubita, T.P. Nyamuhokya, J.J. Komba, H. Ahmed Tanvir, M.I. Souliman, B. Naik, Comparative assessment of the interlayer shear-bond strength of geogrid reinforcements in hot-mix asphalt, Constr. Build. Mater. 191 (2018) 726–735. https://doi.org/10.1016/j.conbuildmat.2018.10.035.
[14] L.F. Walubita, E. Mahmoud, S.I. Lee, G. Carrasco, J.J. Komba, L. Fuentes, T.P. Nyamuhokya, Use of grid reinforcement in HMA overlays – A Texas field case study of highway US 59 in Atlanta District, Constr. Build. Mater. 213 (2019) 325–336. https://doi.org/10.1016/j.conbuildmat.2019.04.072.
[15] S.-H. Yang, I.L. Al-Qadi, Cost-effectiveness of using geotextiles in flexible pavements, Geosynth. Int. 13 (2006).
[16] V.R. Schaefer, Effectiveness of Geotextiles/Geogrids in Roadway Construction; Determine a Granular Equivalent (GE) Factor, 2021.
[17] L.F. Walubita, B.P. Jamison, G. Das, T. Scullion, A.E. Martin, D. Rand, M. Mikhail, Search for a laboratory test to evaluate crack resistance of hot-mix asphalt, Transp. Res. Rec. 2210 (2011) 73–80, https://doi.org/10.3141/2210-08.
[18] L.F. Walubita, T.P. Nyamuhokya, O.L. Torres P., L. Fuentes, H.A. Tanvir, M. Souliman, Laboratory evaluation of grid-reinforced HMA beams using the flexural bending-beam fatigue (FBBF) test in load-controlled mode, Int. J. Pavement Eng. 23 (4) (2022) 1198–1212.
[19] H. Kim, K. Sokolov, L.D. Poulikakos, M.N. Partl, Fatigue evaluation of porous asphalt composites with carbon fiber reinforcement polymer grids, Transp. Res. Rec. 2116 (1) (2009) 108–117.
[20] F. Canestrari, G. Ferrotti, M. Partl, E. Santagata, Advanced testing and characterization of interlayer shear resistance, Transp. Res. Rec. 1929 (2005) 69–78.
[21] D.M.C.-P. Zamora-Barraza, D. Castro-Fresno, A. Vega-Zamanillo, New procedure for measuring adherence between a geosynthetic material and a bituminous mixture, Geotext. Geomembranes. (2010). https://doi.org/10.1016 /j.geotexmem.2009.12.010.
[22] FHWA, Real Cost 2.5, (2010).
[23] Tex-249-F, Test procedure for shear bond strength test, (2021).
[24] Tex-248-F, Test procedure for Overlay Test, (2019).
[25] Python, Python, (2022).
[26] AASHTO-T321-14, Determining the Fatigue Life of Compacted Asphalt Mixtures Subjected to Repeated Flexural Bending, (2014).
[27] AASHTO-T324-11, Hamburg Wheel-Track Testing of Compacted Hot Mix Asphalt (HMA), (2011).
[28] Aashto r50-09, Geosynthetic Reinforcement of the Aggregate Base Course of Flexible Pavement Structures 2009.
[29] B. Evirgen, B. Buyuk, G.T. Cil, T. Deger, Experimental performance of polyester-fiber-based soil geogrids against reflective cracks, Transp. Res. Rec. 2675 (2021) 53–64, https://doi.org/10.1177/03611981211027557.
[30] S. Hu, F. Zhou, T. Scullion, Implementation of Texas Asphalt Concrete Overlay Design System, 2014.
[31] S. Hu, F. Zhou, T. Scullion, Reflection cracking-based asphalt overlay thickness design and analysis tool, Transp. Res. Rec. 2155 (1) (2010) 12–23.
[32] F. Zhou, S. Hu, X. Hu, T. Scullion, Mechanistic-Empirical Asphalt Overlay Thickness Design and Analysis System, 2009.
[33] Z. Fujie, H. Sheng, S. Tom, Overlay tester: A simple and rapid test for HMA fracture property, Road Pavement Mater. Charact. Rehabil. (2022) 65–73. https://doi.org/doi:10.1061/41043(350)9.
[34] G. Montestruque, L. Bernucci, M. Fritzen, L.G. da Motta, Stress relief asphalt layer and reinforcing polyester grid as anti-reflective cracking composite interlayer system in pavement rehabilitation BT - 7th RILEM International Conference on Cracking in Pavements, in: A. Scarpas, N. Kringos, I. Al-Qadi, L. A. (Eds.), Springer Netherlands, Dordrecht, 2012: pp. 1189–1197.
[35] J.G. Collin, T.C. Kinney, X. Fu, Full scale highway load test of flexible pavement systems with geogrid reinforced base courses, Geosynth. Int. 3 (4) (1996) 537–549.
[36] Y. Qian, J. Han, S.K. Pokharel, R.L. Parsons, Stress analysis on triangular-aperture geogrid-reinforced bases over weak subgrade under cyclic loading: an experimental study, Transp. Res. Rec. 2204 (2011) 83–91, https://doi.org/10.3141/2204-11.
[37] A. Zofka, M. Maliszewski, D. Maliszewska, Glass and carbon geogrid reinforcement of asphalt mixtures, Road Mater. Pavement Des. 18 (2017) 471–490, https://doi.org/10.1080/14680629.2016.1266775.